Chemical Engineering Journal 434 (2022) 134771

Contents lists available at ScienceDirect

Chemical Engineering Journal

journal homepage: www.elsevier.com/locate/cej

Determining the kinetic rate constants of Fe_3O_4-to-Fe and FeO-to-Fe reduction by H_2

Qiming Tang, Kevin Huang *

Department of Mechanical Engineering, University of South Carolina, Columbia, SC 29201, USA

ARTICLE INFO

Keywords:
Hydrogen
Iron oxide reduction
Kinetics
Modeling
One-step reduction

ABSTRACT

Steel production using coal accounts for ~ 8% of global carbon emissions. "Green Steel" is a new grand concept proposed recently to make steel from iron ores using renewable derived "Green Hydrogen" to achieve zero carbon emission. The kinetics and rate-limiting steps of iron ore reduction into iron with H_2 as a reducing agent is critically important to the success of this new technology. While reduction of Fe_2O_3 into Fe by H_2 follows multiple steps, the past research on this topic mainly deals with the overall averaged kinetics, giving little information on the elemental and rate-limiting steps. Here we report a kinetic study specifically design to attain kinetic rate constants of one-step reduction of Fe_3O_4-to-Fe and FeO-to-Fe. Guided by thermodynamics, we show first how to create in situ the desirable starting oxide phases, i.e., Fe_3O_4 and FeO, with precisely controlled the ratio of partial pressures of H_2O and H_2. We then show time-dependent raw H_2O content data collected by a mass spectrometer and the processed reduction data to extract kinetic rate constants. We found that the kinetics of the two one-step reduction reactions follows nicely the Johnson-Mehl-Avrami (JMA) phase transformation model. The one-step reduction mechanisms and activation energy are also discussed.

1. Introduction

Reduction kinetics of iron ores to metal iron by coke is one of the most studied subjects in metallurgy of the past century [1–6]. The early extensive research has provided foundational database for modern iron and steelmaking industry. As concerns on global warming and climate change are mounting in recent decades, this old and carbon emission intensive steelmaking process is currently under scrutiny for carbon footprint reduction. One attractive solution proposed recently is to use H_2 produced from renewable energy, or so-called green H_2, to reduce iron ores into iron with only steam as the emission product (thus zero carbon emission footprint) [7–8]. This proposal is currently gaining significant interest from industry as the carbon tax is being considered and the price of green H_2 is falling with the rapid advancement in water electrolysis technology in recent years. Therefore, studying reduction kinetics of iron ores into iron by H_2 has received a renewed interest.

There are ample kinetic studies on the reduction kinetics of iron ores to iron by H_2 in the literature [9–14]. However, most of these studies dealt with the total reduction of Fe_2O_3 (raw iron ore) to Fe. Thermodynamics indicates that Fe_2O_3 reduction into Fe takes multiple steps. Above 550 °C, Fe_2O_3 is first reduced into Fe_3O_4, then FeO and finally Fe. Below 550 °C, Fe_2O_3 is first reduced into Fe_3O_4, and then Fe. Those early kinetic studies did not consider the individual reduction steps, but a lump sum of all intermediate steps [15–19]. Thus, the obtained kinetic data represent an average of the individual sequential reduction steps without the information on the rate limiting steps (RLS).

At the same time, reduction of iron oxide into iron by H_2 is also an important half reaction for chemical looping H_2 (CLH), a thermochemical process that can produce H_2 with high purity and high efficiency at large scale [20–22]. It is also a core reaction for the recently developed solid oxide iron-air batteries (SOIAB) operated on oxide-ion chemistry [23–27]. Therefore, a detailed elucidation on the kinetics of iron oxide reduction by H_2, particularly that of single-step reduction, such as Fe_3O_4 to Fe and FeO to Fe, is of significant interest to both scientific community and industrial engineering toward "green steel" technology.

Here we report a specially designed study on kinetics of one-step FeO_x-to-Fe reduction using H_2 as a reducing agent. To enable the one-step reduction, the starting phase of iron oxide is critical. We, based on Baur-Glaessner's equilibrium diagram of Fe-O–H system, use a H_2-H_2O-Ar mixture with a precisely controlled H_2O/H_2 ratio to *in-situ* synthesize the desired starting iron oxide, on which reduction kinetic study is carried out under different H_2 concentrations and temperatures.

* Corresponding author.
E-mail address: huang46@cec.sc.edu (K. Huang).

https://doi.org/10.1016/j.cej.2022.134771
Received 30 October 2021; Received in revised form 10 January 2022; Accepted 14 January 2022
Available online 20 January 2022

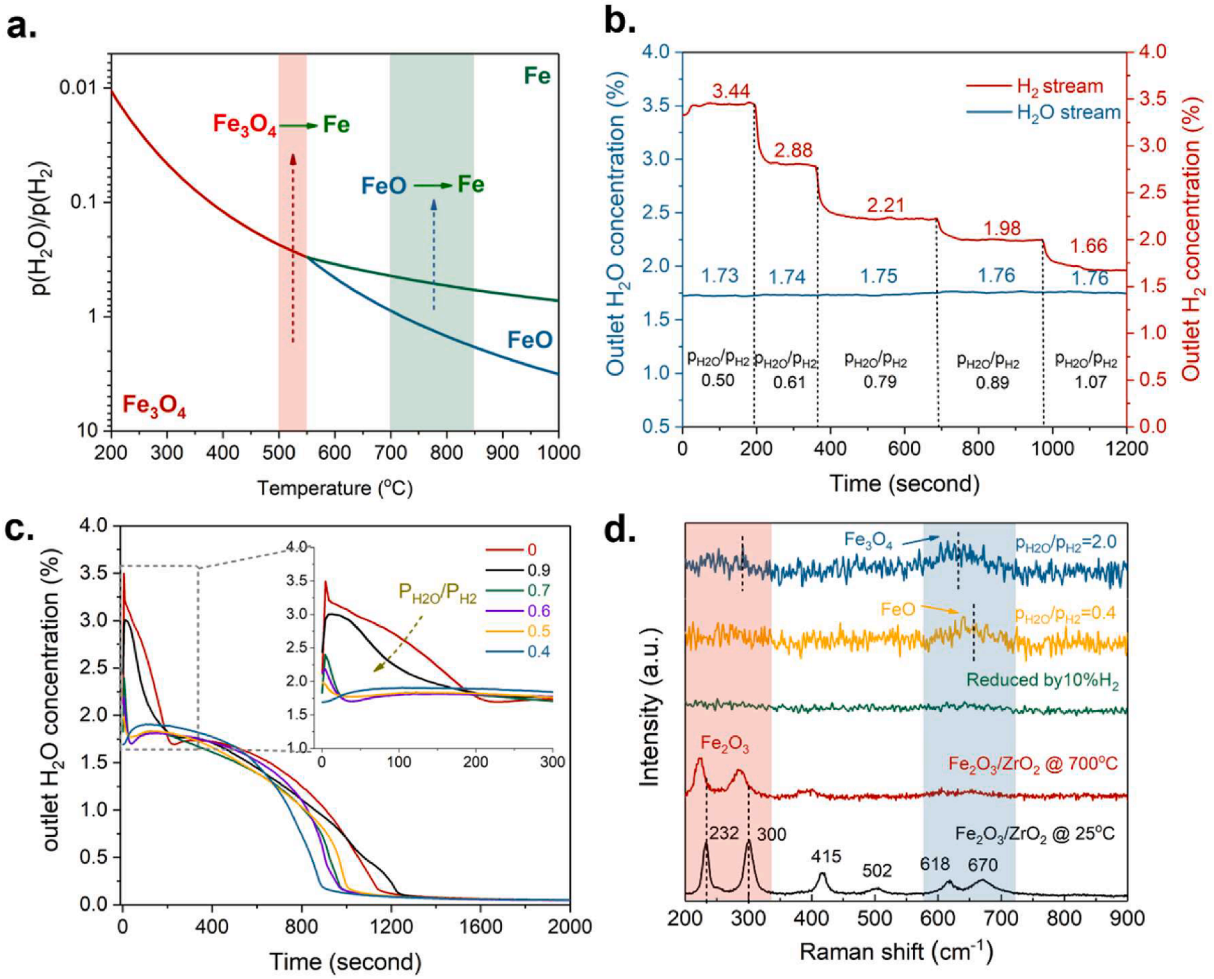

Fig. 1. (a) Baur-Glaessner's equilibrium diagram of the Fe-O–H system calculated by HSC Chemistry 6.0. (b) The ratio of H_2O and H_2 analyzed by MS corresponding to the change of H_2 flow rates. (c) The profiles of the outlet gas composition during reduction process in 10% H_2 at 700 °C for different starting states of reduction. (d) *In-situ* Raman spectra of Fe_2O_3/ZrO_2 sample in different gas environments.

Using the *in-situ* formed FeO_x for the reduction kinetic study is simple and efficient compared to the conventional methods using a starting oxide; the latter must be maintained properly during heating by controlling partial pressure of oxygen in the surrounding atmosphere.

2. Experimental and methods

2.1. Apparatus and materials

The setup for kinetic study of iron oxides has been previously described [11], see Figure S1. The only modification for this study was the replacement of a steam generator/water pump by a water bubbler to ensure a more stable steam supply at the low concentration range. The described H_2O/H_2 ratio was then simply controlled by the mass flow rates of the add-in H_2. The original starting iron oxide is Fe_2O_3 mixed with ZrO_2 to minimize any Fe-sintering during the study. The Fe_2O_3/ZrO_2 composite in a molar ratio of Fe:Zr = 85:15 was prepared by a co-precipitation method. Briefly, the stoichiometric solutions of $Fe(NO)_3{\cdot}9H_2O$ (≥99.999%, Sigma-Aldrich) and $ZrO(NO)_2{\cdot}xH_2O$ (≥99.999%, Alfa-Aesar) were first dissolved in deionized water separately. Then the two solutions were mixed in a beaker with a cation concentration of 0.1 M. The resultant clear orange solution was then added dropwise to an ammonium carbonate solution bath under a constant stirring. To ensure a full precipitation of all the cations in the solution, the molar ratio of $(NH_4)_2CO_3$ (Sigma-Aldrich) and M^{n+} (M = Zr and Fe) was kept as $n(NH_4)_2CO_3{:}nM^{n+}$=2.5:1. The resultant brownish precipitate was then left in the solution for 20 h with continuous stirring. Finally, the aged suspension was filtered and washed several times with ethanol, dried overnight at 80 °C and calcined in air at 600 °C for 5 h to yield the final product. We have previously emphasized the importance of mixing ZrO_2 with iron oxides to obtain reliable kinetic data due to the excellent resistance of ZrO_2 to Fe-particles sintering [11].

2.2. Materials characterization

The phase composition of the prepared Fe_2O_3/ZrO_2 composite was examined by X-ray diffraction (Rigaku D/MAX-2100). The surface compositions of Fe_2O_3/ZrO_2 upon exposure to H_2O/H_2 mixture under different H_2O/H_2 ratios and temperatures were also probed by a Xplora plus Raman spectrometer (HORIBA) equipped with a commercial Linkam TS 1000 heating stage (Figure S2). Roughly 0.1 g Fe_2O_3/ZrO_2 powders were placed into a crucible on the heating stage and gently pressed with a glass rod to obtain a flat surface. Figure S2a shows schematically a quartz window, sealed with Buna O-ring, used to allow transmission of the excitation laser and collection of scattered photons. The stainless-steel jacket of the gas-stream chamber was cooled with a circulating water. Figure S2b-2e show the setup of *in-situ* Raman testing system. The lens with 50 × magnification and long working distance (8 mm) objective were used with laser excitation in wavelength of 638 nm. The Raman spectra were collected using the LabSpec 6 software every 3 min. The morphologies of the Fe_2O_3/ZrO_2 before and after reaction were also captured by a field emission scanning electron microscope (FESEM,

Zeiss Gemini500).

2.3. One-step reduction experiment

The reduction kinetic data were collected in the same way as previously described [11]. In the current modified system, the steam was controlled by a bubbler at room temperature instead of a steamer, which will provide a fixed H_2O content to the carrier gas Ar. Briefly, the experiment was started by first loading 100 mg Fe_2O_3/ZrO_2 into a quartz tube reactor, following by raising furnace temperature to 400 °C under Ar at 200 cm^3/min. Then, a 10% H_2-Ar was introduced into the reactor chamber during temperature ramp to the target point, i.e., 500, 525, 550, 700, 750, 800 and 850 °C. The effluent was constantly analyzed by an online mass spectrometer (MS) during reduction and a full reduction of the Fe_2O_3 into Fe is confirmed by the H_2 concentration, i.e., there will be no H_2 consumption upon full reduction. After this initial full-reduction activation process, the oxidation was carried out by switching to a gas with a controlled H_2O/H_2 ratio to achieve a desirable oxide form. To control the H_2O/H_2 ratio, H_2 with a fixed mass flow rate is added into the room-temperature moistened Ar stream at a fixed flow rate. We use Fig. 1a of thermodynamic phase diagram as a guidance to dial a H_2O/H_2 ratio for a specific iron oxide. For example, P_{H2O}/P_{H2} = 0.4 was set for FeO at 700–850 °C, whereas P_{H2O}/P_{H2} = 2.0 was set for Fe_3O_4 at 500–550 °C. Once the wanted oxide phase is realized, the one-step reduction, viz. Fe_3O_4 to Fe and FeO to Fe, was performed at different H_2 concentrations in Ar (5%, 10% and 20%). The reduction kinetics was evaluated based on the change in H_2O concentration in the effluent measured by MS.

3. Results and discussion

3.1. Confirmation of the starting oxide for H_2-reduction

Fig. 1a shows the Baur-Glaessner's equilibrium diagram of the Fe-O–H system represented as a function of temperature and partial pressure ratios of H_2O and H_2 (P_{H2O}/P_{H2}). The diagram indicates the following phase domains: Fe, FeO and Fe_3O_4. At low temperature (T < 550 °C), only metallic Fe and Fe_3O_4 are in equilibrium with H_2-H_2O gas phase, meaning that Fe_3O_4 can be directly reduced into Fe by H_2 through a single step. In contrast, there is an intermediate phase of FeO before Fe_3O_4 is fully reduced to Fe at T ≥ 550 °C. To study the kinetics of a specific one-step reduction process at T ≥ 550 °C, the P_{H2O}/P_{H2} is precisely controlled to achieve FeO, see the short line in Fig. 1a. In this study, we focus on two temperature ranges of 500–550 and 700–850 °C, where Fe_3O_4 to Fe and FeO to Fe reduction reactions are prevalent, respectively.

To precisely control the H_2O content, we first performed a calibration on H_2O content. Fig. 1b shows the ratio of H_2O and H_2 in the reaction chamber analyzed by MS with a room-temperature water bubbler. The H_2O concentration in effluent was found to be 1.75%, less than the theoretical 3.13%, which implies that the saturation of Ar by H_2O is not perfect with the bubbler. With the known H_2O content, the H_2 flow rate can be accordingly set to achieve the desirable H_2O/H_2 ratio and thus the wanted starting iron oxide phase for reduction kinetic study. Fig. 1c shows an exemplary profile of the outlet H_2O concentration variation during the reduction process in 10% H_2-Ar at 700 °C on a sample treated in different P_{H2O}/P_{H2} ratios, thus with different oxide phases. According to Fig. 1a, there exists two possible iron oxide phases at 700 °C: Fe_3O_4 and FeO, depending on the ratio of P_{H2O}/P_{H2}. Without H_2O, the starting iron oxide has been previously confirmed as Fe_3O_4 due to the residual oxygen in Ar [11], which will have to go through FeO first before being fully reduced into Fe. Thus, the total reduction process includes two steps: Fe_3O_4 to FeO and then FeO to Fe. The first hump before 200 s is a characteristic of such a two-step reduction process. We have previously studied this two-step combined reduction kinetics [11]. However, the main objective of this study is to obtain kinetic rate constants of one-step direct reduction such as FeO to Fe and Fe_3O_4 to Fe. As shown in Fig. 1c, as we decrease P_{H2O}/P_{H2} ratio (moving from bottom up in the inset) from 0.9 to 0.4, the first hump disappears abruptly at $P_{H2O}/P_{H2} \leq 0.7$, implying that starting oxide phase for reduction becomes FeO. To ensure FeO is free of Fe_3O_4, we use P_{H2O}/P_{H2} = 0.4 for FeO formation.

To independently confirm the phase formed is what we want, we also performed *in-situ* Raman spectroscopy on sample exposed to different gases; they are shown in Fig. 1d. The spectrum of Fe_2O_3/ZrO_2 at room temperature (black) exbibits distinct Raman shifts at 232 (A_{1g}), 300 (E_g), 415 (E_g), 502 (A_{1g}), 618 (E_g) and 670 cm^{-1} (LO E_u), assigned to the hematite's irreducible vibrational modes [28]. While there is no obvious Raman peak for ZrO_2, its presence is confirmed by XRD pattern shown in Figure S3. Compared to the Raman spectra of prepared Fe_2O_3/ZrO_2 powders at room temperature, all peaks collected at 700 °C are slightly red-shifted (red) since the lattice expansion of Fe_2O_3 at high temperatures decreases the vibration frequency of Fe-O bonds. The variations of Raman spectra with gas environments at 700 °C are shown in Fig. 1d, marked with green, orange, and blue. After a full exposure to 10% H_2-Ar, all Raman peaks disappeared, suggesting the Fe_2O_3 has been fully reduced to metallic Fe. After we introduced a wet H_2 with P_{H2O}/P_{H2} = 0.4, a wide but weak peak at 600–700 cm^{-1} appears, which can be assigned to FeO [29]. When P_{H2O}/P_{H2} is increased to 2.0, additional peak at 650 cm^{-1} corresponding to Fe_3O_4 appears [30]. Compared to the standard Raman active phonon modes for FeO and Fe_3O_4 phases [28], all of Raman peaks shows slightly red shift because of the high temperature. The small weak peaks at 250 and 300 cm^{-1} observed at P_{H2O}/P_{H2} = 2 and 700 °C might suggest a trace amount of Fe_2O_3 also formed under this condition. Compared to using pure FeO and Fe_3O_4 for a similar study, employing the *in-situ* formed FeO_x for the reduction kinetic study is simple, efficient, and accurate.

3.2. Kinetics models

The reduction process of iron oxide with H_2 usually involves a sequence of nucleation and growth steps. Johnson-Mehl-Avrami (JMA) solid-state phase transformation model has been widely and universally used to describe such an isothermal reduction kinetics [6,16,19,31–37]. In this model, a new phase is nucleated by germination nuclei contained in the old phase, followed by growth. The JMA equation relates the transformed fraction at a constant temperature T and reaction time t. Once ξ is determined, the overall kinetic rate *k(T)* can be calculated by:

$$\xi(t) = 1 - exp[-k(T)t^n] \quad (1)$$

where t is the reaction time, ξ is the reduction extent, $k(T)$ is the Arrhenius rate constant, which can be given by $k(T) = A^*\exp\left(-\frac{E_a}{RT}\right)$ and n is the Avrami exponent that depends on the mechanism of nucleation and growth process [38]. Generally, $n = \lambda + \beta$, where λ is the dimensionality of growth, $\lambda = 1, 2 or 3$; and β depends on the nucleation process ($0 < \beta < 1, \beta = 0$ represents instantaneous nucleation and $\beta = 1$ means a very slow nucleation rate).

Using the logarithmic form and rearrangement of eq. (1), Sharp-Hancock equation can be derived [32]:

$$ln[-\ln(1-\xi)] = nln(t) + \ln(k) \quad (2)$$

The local $n(\xi)$ can be calculated by differentiating eq. (2) into:

$$n(\xi) = \frac{\partial \ln(-\ln(1-\xi))}{\partial \ln(t)} \quad (3)$$

In addition, during the iron oxide reduction process, the reaction rates can be also expressed by:

$$\frac{d\xi}{dt} = k(T)^* f(\xi) \quad (4)$$

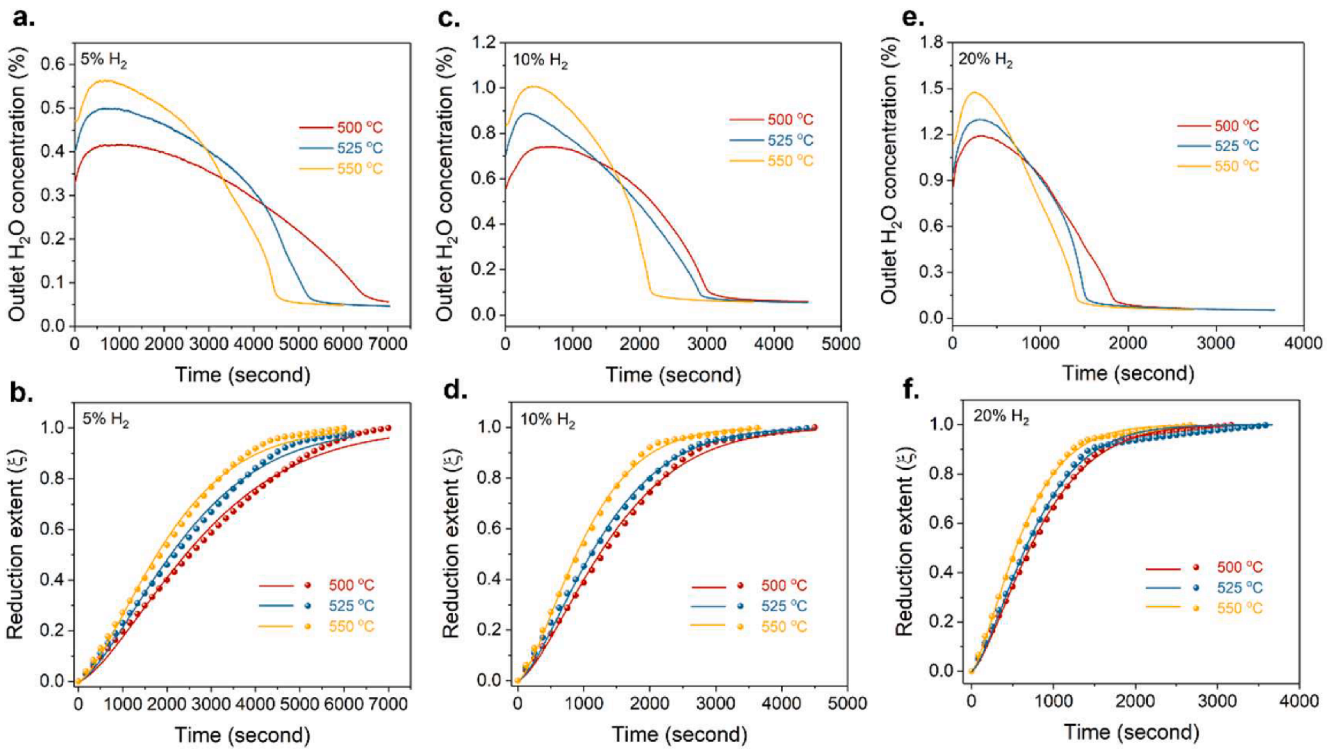

Fig. 2. Reduction kinetic data: profiles of outlet water concentration changes during reduction process and corresponding reduction extent (dot) of Fe_3O_4 versus time and JMA reduction model fitting curves (line) at 500 to 550 °C in (a and b) 5% H_2, (c and d) 10% H_2, and (e and f) 20% H_2.

where $f(\xi)$ is the integration reaction model function. For the reduction kinetics under isothermal conditions, eq. (4) can be integrated into:

$$g(\xi) = \int_0^{\xi} \frac{d\xi}{f(\xi)} = kt = A^* exp\left(-\frac{E_a}{RT}\right)t \tag{5}$$

where $g(\xi)$ is the function of the integration reaction model function. By taking the logarithm and rearranging eq (5), one can get:

$$\ln(t) = (-lnA + lng(\xi)) + \frac{E_a}{RT} \tag{6}$$

where t is the time for a specific reduction extent. By plotting $\ln(t)$ versus $1/T$ based on the eq. (6), the activation energies E_a can be obtained at different reduction extents.

3.3. Reduction kinetics of Fe_3O_4 to Fe

The isothermal kinetics of Fe_3O_4 to Fe reduction process in H_2-Ar was determined by measuring the variations of H_2O content in the effluent and subsequent data processing with JMA model. The change in H_2O concentration vs. time during the reduction process is due to oxygen removal from iron oxide. Fig. 2a, 2c, 2e show the outlet H_2O content variations with time-on-reduction from 500 to 550 °C under different inlet H_2 concentrations, while Fig. 2b, 2d, 2f show the corresponding normalized degree of Fe_3O_4 reduction vs. time. It is evident that the reduction kinetics is affected by both of temperature and H_2 concentrations. Compared to multiple step reduction process in our previous report [11], there is nearly no peak related to Fe_3O_4 to FeO reduction, suggesting the one-step reduction of Fe_3O_4 to Fe has been achieved under this condition.

The results also show that the H_2O production is faster in the early stage than the later one. To determine the kinetic rate constant, JMA model was applied to fit the experimental data, see lines in Fig. 2b, 2d and 2f. The sigmoidal profile of these kinetic plots could be divided into three periods based on JMA model [32]: (1) induction period ($0 < \xi <$ 0.05); (2) acceleration region ($0.05 < \xi < 0.8$); (3) deceleration period and completion ($0.8 < \xi < 1.0$); The induction period tends to be dominated by nucleation events, while the acceleration region can be attributed to the growth of the new phase and the deceleration region is associated with the coalescence of Fe and thus affecting the diffusion. At a given temperature, values of k, n and E are extracted from the fitting results, which are summarized in Table S1. The n value is found to be constant at 1.45, indicating that a 1-diamensional nucleation and growth process for the reduction. The Arrhenius plots of k are shown in Fig. 3, from which E_a are obtained to be 47.6 ± 2.8, 50.6 ± 5.6 and 40.1 ± 2.3 kJ mol^{-1} for 5, 10 and 20% H_2, respectively. The weak dependence of E_a on H_2 concentration infers that energy barrier of the reduction process may not be mass transfer limited.

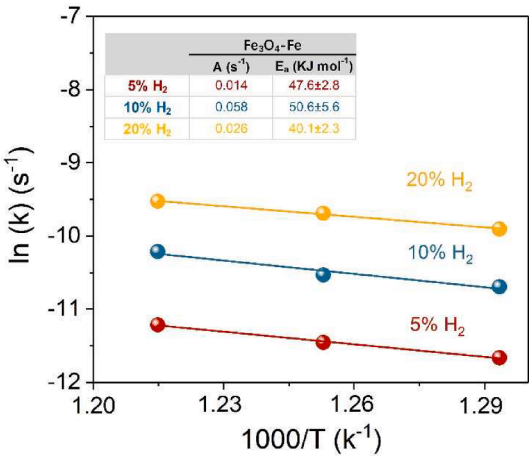

Fig. 3. Arrhenius plots of rate constant of Fe_3O_4 to Fe reduction derived from the JMA phase transformation model.

To evaluate the order of solid-state reaction rate for the one-step

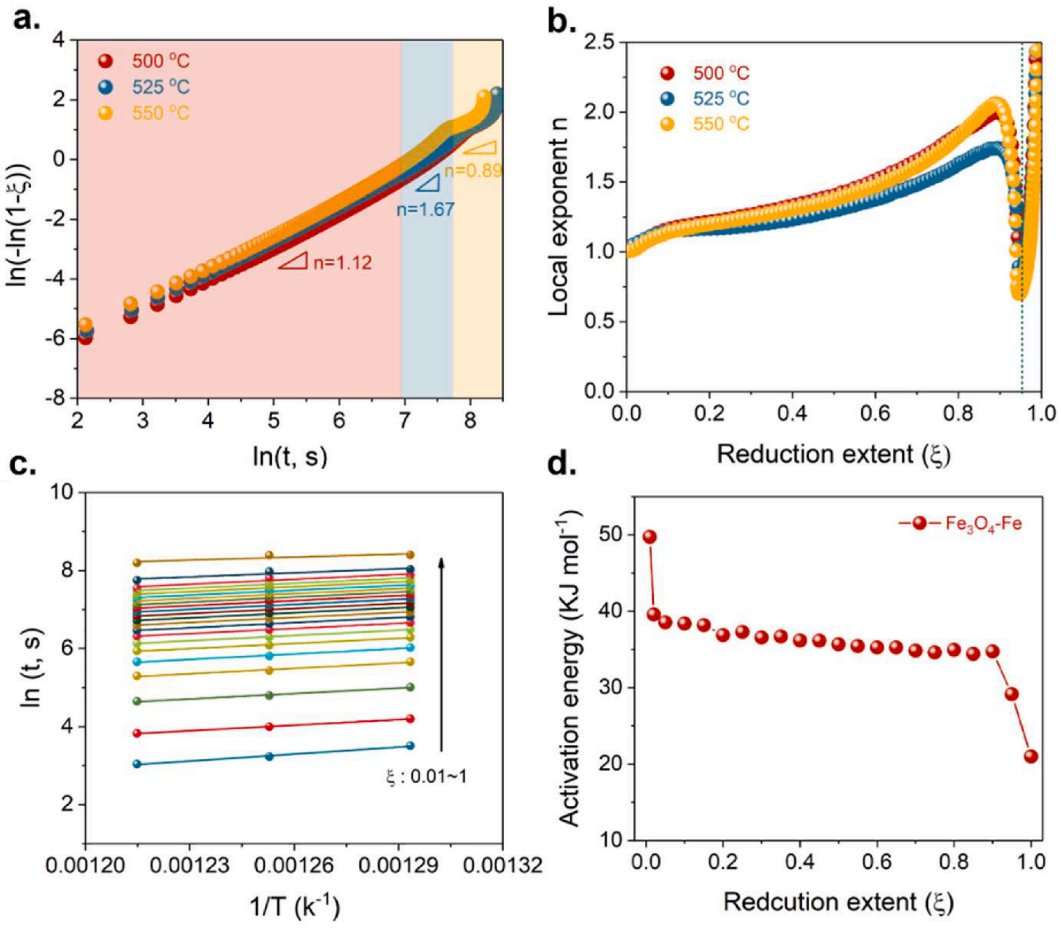

Fig. 4. (a) Sharp-Hancock plots of ln(-ln(1-ξ)) vs. ln (t) based on the data at 500 to 550 °C in 10% H_2. (b) local exponent n values vs. reduction extent at 500 to 550 °C in 10% H_2. (c) ln (t) vs. 1/T with different reduction extents at 500 to 550 °C in 10% H_2. (d) Activation energy as a function of the reduction extent for the conversion of Fe_3O_4 to Fe.

reduction, Sharp-Hancock plots of ln(-ln(1-ξ)) vs. ln (t) based on the actual experiment data are shown in Fig. 4a at 500 to 550 °C in 10% H_2. There are apparently three distinct stages with different Avrami exponents n in the whole conversion process. At the beginning of the conversion, the average of n value is ~ 1.12; at the medium state, the n increases to ~ 1.67; at the final stage, n decreases to 0.89. It is worth noting that when the reduction extent is close to 1, n trends to be infinite, which is attributed to the boundary conditions of the mathematical function ($\xi \neq 1$ in eq. (3)). The variation of Avrami exponent n during the reduction reaction indicates that there are different dominating mechanisms in each reaction stage. To explore local exponent n at different reduction extent, using eq. (3), local exponent n vs. reduction extent ξ are plotted and shown in Fig. 4b. At the beginning of reaction, the n-value increases and reaches a maximum value, suggesting the one-dimensional (1D) growth with a decrease in the nucleation rate, which agrees with the results in Fig. 4a. At the end of reduction, the n falls below 1, implying that the reduction process becomes diffusion-controlled, possibly due to the blocking effect of partially sintered Fe particles. To further provide a clearer picture of the mechanisms, with eq. (6), the plots of ln (t) vs. 1/T obtained at $\xi = 0.01$ to full reduction ($\xi = 1$) from 500 to 550 °C in 10% H_2 are shown in Fig. 4c. For a given reduction extent ξ, E_a can be obtained from the slope of each line. Fig. 4d plots the derived E_a vs. ξ, which shows E_a decreases with reduction extent. This trending can be explained according to the crystal nucleation and growth theory by the fact that E_a required during nucleation is higher than that of new-phase growth [37]. Therefore, the reduction kinetics of Fe_3O_4 to Fe follows the nucleation and growth model.

To observe the change in morphologies of the specimen before and after reduction and to ensure that mass transport is not a serious issue for the study, SEM images of the original Fe_2O_3/ZrO_2 before and after reduction at different temperatures were collected; they are shown in Fig. 5.

Fig. 5a is a typical SEM image of the as-prepared Fe_2O_3/ZrO_2 before reduction, consisting of uniform spherical nanoparticles with an average particle size of 30 nm. After reduction at 500 °C to 550 °C, Fig. 5b-5d show some minor degree of agglomerations with an average particle size of 200 nm. But there are still some nanoparticles (few nanometers) visibly anchored on the surface of larger particles. The elemental mapping on the reduced sample shown in Fig. 5e-5i cannot conclusively identify the real compositions of these nanoparticles due to the resolution issue of EDX. In other words, these nanoparticles could be pure Fe or Fe-oxide.

3.4. *Reduction kinetics of FeO to Fe*

The kinetics of FeO to Fe reduction taking place above 550 °C is equally important to that of Fe_3O_4 to Fe from both scientific and engineering perspectives. However, there are scarce reports in the literature dealing with the kinetics of this single-step reduction. We here apply similar method to the study of Fe_3O_4-Fe reduction. The starting FeO was obtained by controlling the P_{H2O}/P_{H2} as described above. The collected raw data and converted reduction extent ξ are shown in Fig. 6a-6f. The FeO-Fe one-step reduction can be confirmed by the single reduction peak in Fig. 6a, 6c and 6e. With the JMA model, the fitting results are plotted as lines in Fig. 6b, 6d and 6f. The extracted n, k and E_a values are summarized in Table S2. The average n value is close to 1.45, indicating

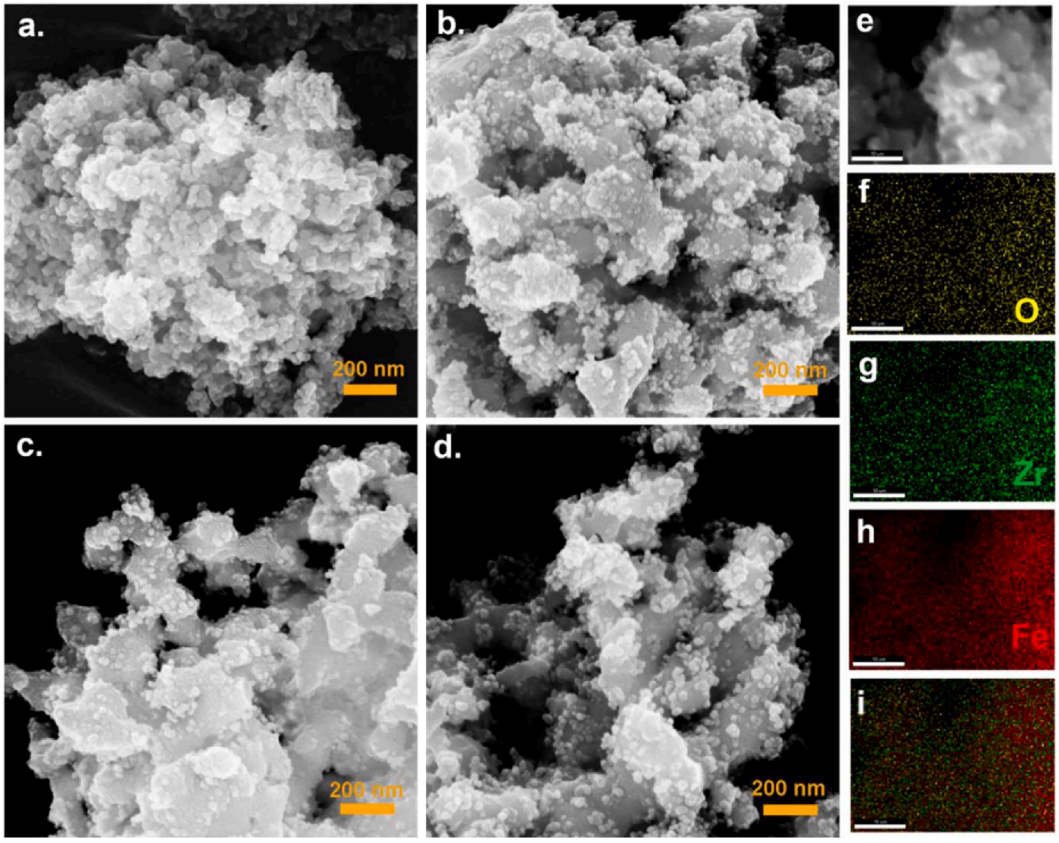

Fig. 5. SEM images of (a) pristine Fe_2O_3/ZrO_2 before reduction; after reduction in 10% inlet H_2 at (b) 500, (c) 525 and (d) 550 °C. (e) Area of element mapping of reduced sample at 550 °C for (f) O, (g) Zr, (h) Fe and (i) overlay of different elements.

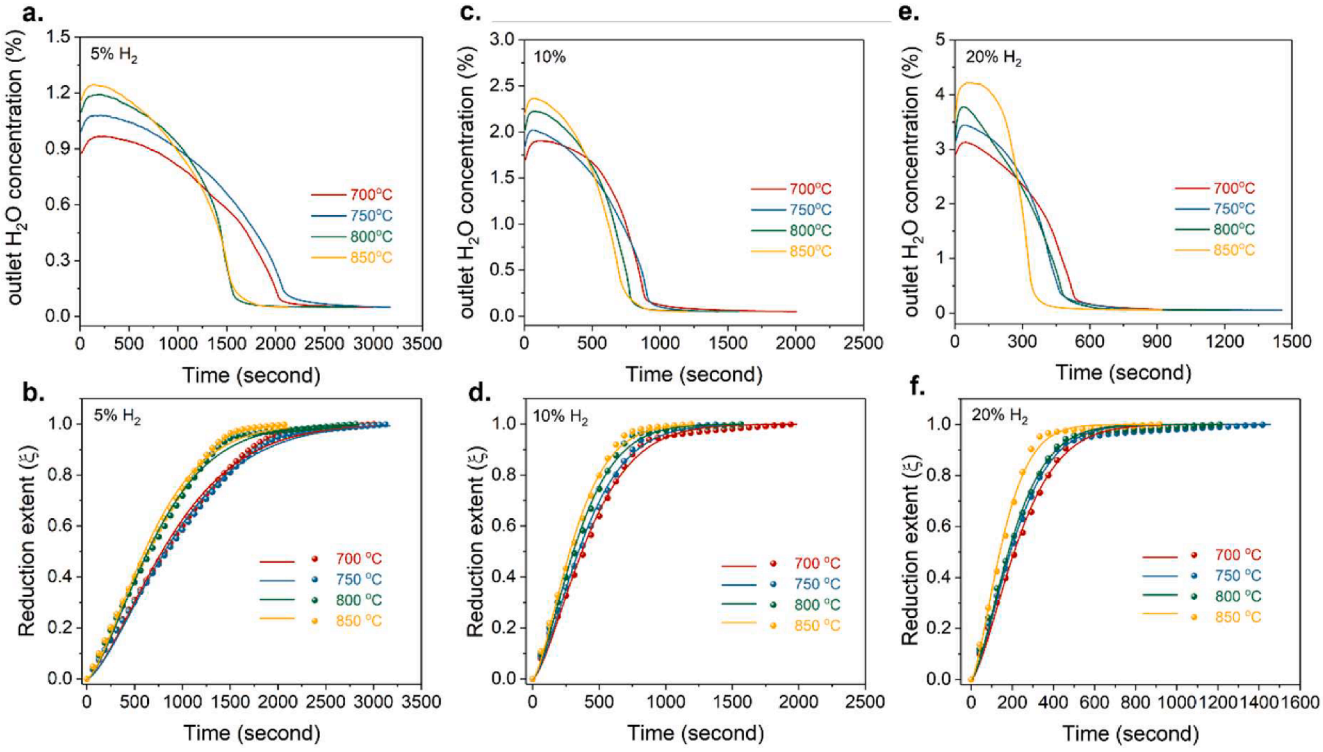

Fig. 6. Profiles of outlet H_2O concentration during reduction process and corresponding reduction extent (dot) vs. time with JMA model fitting curves (line) from 700 to 850 °C in (a and b) 5% H_2, (c and d) 10% H_2, and (e and f) 20% H_2.

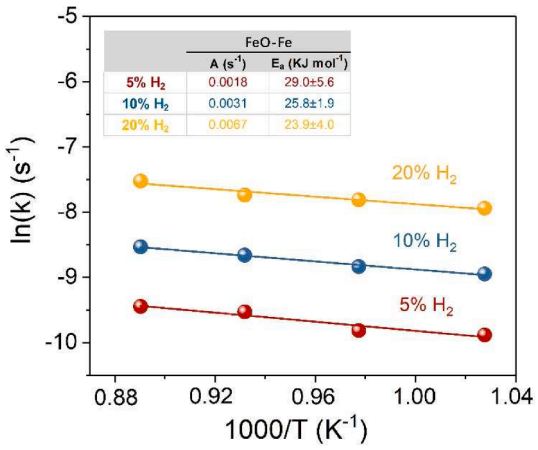

Fig. 7. Arrhenius plots of rate constant of FeO to Fe reduction derived from the JMA phase transformation model.

that a 1-diamensional nucleation and growth process. The Arrhenius plots of k is shown in Fig. 7, from which E_a are obtained to be 29.0 ± 5.6, 25.8 ± 1.9 and 23.9 ± 4.0 KJ mol^{-1} for 5, 10 and 20% H_2, respectively. The E_a has a weak dependence on H_2 concentration and is smaller than that Fe_3O_4-Fe reduction. Compared to the Fe_3O_4-Fe reduction, the rate constant of FeO-Fe reduction is roughly two orders of magnitude higher than that of Fe_3O_4-Fe reduction, largely due to the higher temperatures and possibly lower oxygen content or diffusion-friendly defects present in FeO.

To further investigate the one-step FeO-Fe reduction mechanisms, n value describing the phase transformation is discussed. Sharp-Hancock plots for the FeO-to Fe reduction are shown in Fig. 8a. It is evident that the Avrami exponent n for the overall reduction process is not a constant. At the beginning of the reduction, n value is averaged at 1.09; in the intermediate stage, n increases to ~ 1.63; in the final stage, n decreases to 1.01. The variations of Avrami exponent n with the extent of reduction ξ imply that the dominating mechanisms are changing with reaction stages. To explore local exponent n at different reduction extent ξ, using eq. (3), we plot local exponent n values with reduction extent ξ in Fig. 8b. Like the Fe_3O_4-Fe reduction shown in Fig. 4b, at the beginning of transformation, n increases to 2.5, corresponding to a growth mechanism changing from 1D to 2D, but decreases to ~ 0.5 at the end of reduction, suggesting a decrease in the nucleation and growth rate. This trending can be attributed to the diffusion limitation induced by the partial sintering of Fe particles at high temperatures. To further provide a clearer picture of the mechanisms, using eq. (6), we plot ln (t) vs. 1/T in Fig. 8c at ξ = 0.05 to full reduction (ξ = 1) at 700–850 °C in 10% H_2. At a given reduction extent ξ, E_a can be obtained from the slope of a fitting line for the plots. Fig. 8d shows the derived E_a vs. ξ. The results clearly indicates that E_a decreases with reduction, which can be explained by the fact that E_a required during the initial nucleation is higher than that of growth. But in the intermediate stage, E_a keeps roughly constant at ~ 17 kJ mol^{-1}, implying the nucleation and growth of FeO-Fe reduction becomes homogeneous.

The morphologies of the specimen after reduction at high temperatures are shown in Fig. 9 of SEM images. After reduction at 700 to 850 °C, some agglomerations are observed in comparison to the original

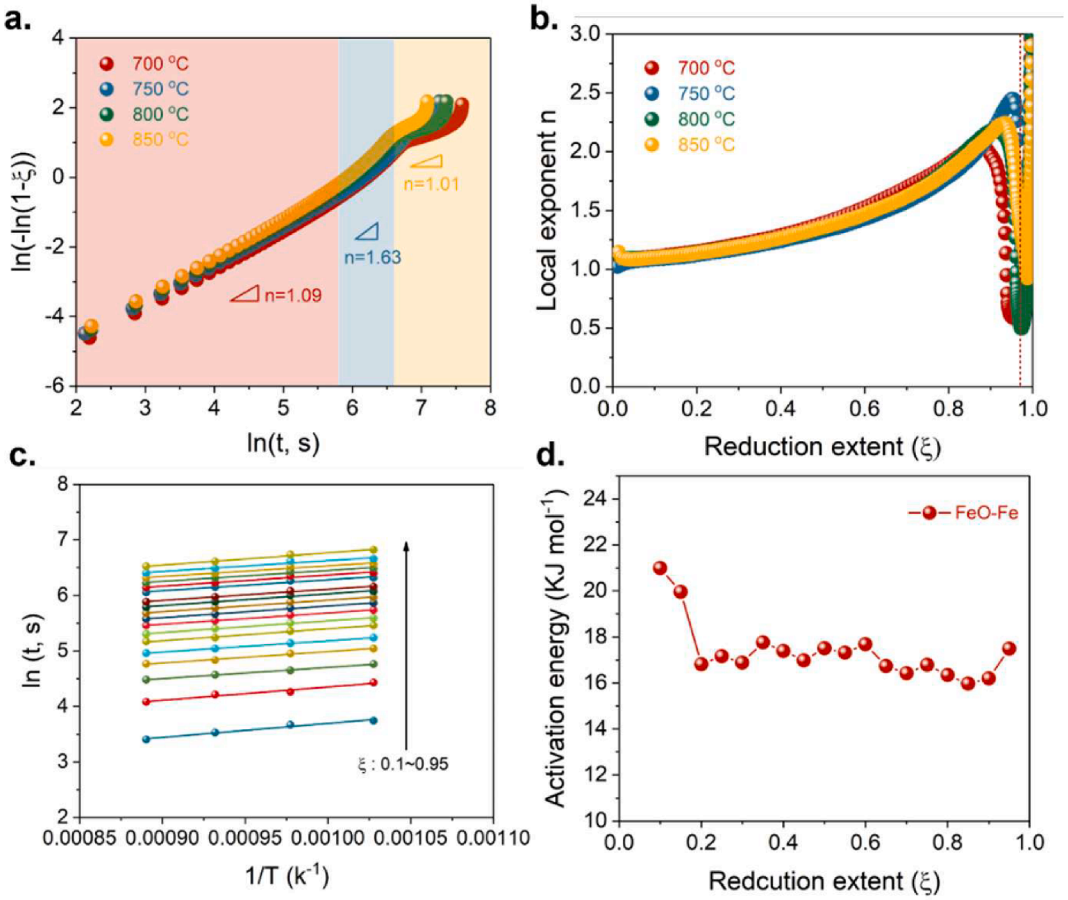

Fig. 8. (a) Sharp-Hancock plots of ln(-ln(1-ξ)) versus ln (t) based on the measurement data at 700 to 850 °C in 10% H_2. (b) local exponent n vs. reduction extent at 700 to 850 °C in 10% H_2. (c) plots of ln (t) vs. 1/T with different reduction extents at 700 to 850 °C in 10% H_2. (c) Activation energy vs. reduction extent for the conversion of FeO to Fe.

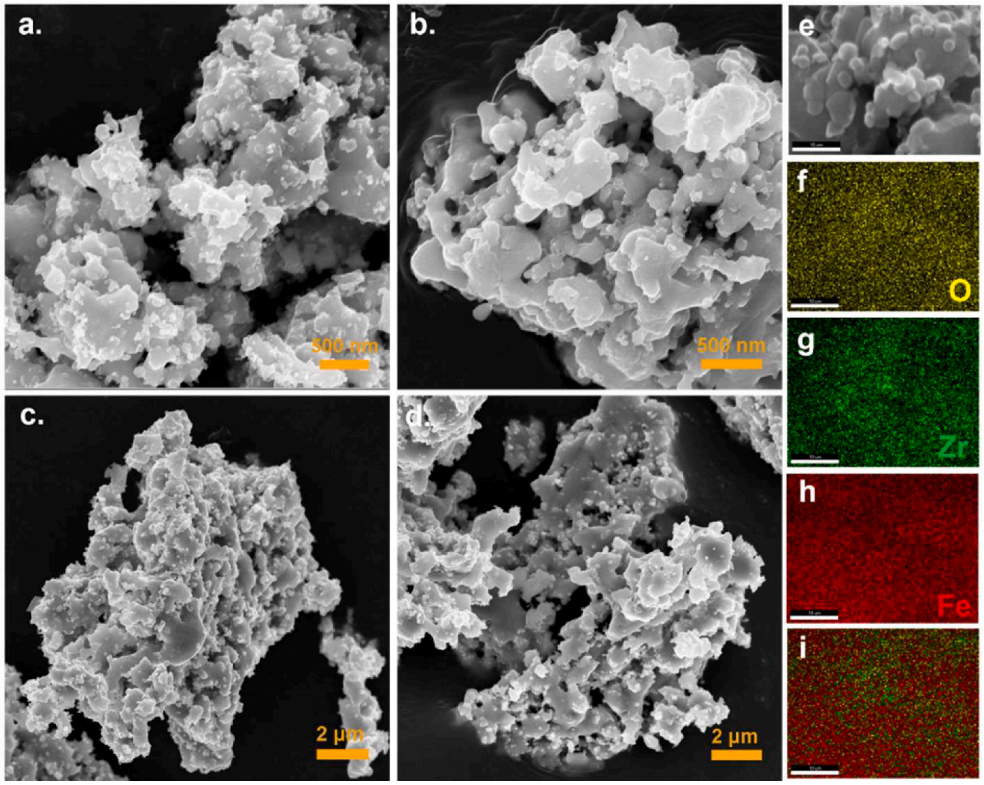

Fig. 9. SEM images of Fe_2O_3/ZrO_2 after reduction in 10% inlet H_2 at (a) 700, (b) 750, (c) 800 and (d) 850 °C. (e) area of element mapping of reduced sample at 700 °C for (f) O, (g) Zr, (h) Fe and (i) overlay of different elements.

morphologies (Fig. 5(a)) of Fe_2O_3/ZrO_2 before reduction as well as those exposed to intermediate temperature reduction (Fig. 5b-5d). These agglomerations could result in a slowed kinetics at the final state of reductions even though ZrO_2 as sintering inhibitor is present and has a homogenic distribution (Fig. 9e-9i). However, compared to ZrO_2-free iron oxide reduction, the sintering is marginal.

4. Conclusion

In summary, we have shown that the desired iron oxide, Fe_3O_4 or FeO, can be formed *in-situ* from fully reduced iron particles by precisely controlling the ratio of H_2O and H_2 concentrations at a given temperature. With the desired iron oxide, the reduction kinetics of one-step iron oxide to iron has been studied by measuring H_2O content vs. time with an on-line mass spectrometer and phenomenological modeling. It is found that the reduction degree of the two one-step reduction reactions follows nicely the Johnson-Mehl-Avrami (JMA) phase transformation model, revealing three stages during the reduction, in which the E_a of the nucleation is faster than the growth. From the kinetics analysis, the Fe_3O_4 to Fe reduction was shown to be 1D growth with a decrease in the nucleation rate, while the FeO to Fe reduction shows a faster growth mechanism changing from 1D to 2D. In addition, the kinetics of FeO to Fe reduction exhibits two orders of magnitude higher kinetic rate constant than that of Fe_3O_4 to Fe counterpart with half the activation energy of the latter. This work provides an in-depth explanation for the process of FeO to Fe and Fe_3O_4 to Fe reduction, and foundational data for engineering and design of practical CLH and SOIAB.

Declaration of Competing Interest

The authors declare that they have no known competing financial interests or personal relationships that could have appeared to influence the work reported in this paper.

Acknowledgements

We would like to thank National Science Foundation for the financial support under award number 1801284 and Department of Energy, Office Fossil Fuels, National Energy technology Laboratory for the financial support under award number DE-FE-0031671.

Appendix A. Supplementary data

Supplementary data to this article can be found online at https://doi.org/10.1016/j.cej.2022.134771.

References

[1] Z. Liang, L. Yi, Z. Huang, B. Huang, H. Han, A novel and green metallurgical technique of highly efficient iron recovery from refractory low-grade iron ores, ACS Sustainable Chem. Eng. 7 (22) (2019) 18726–18737.
[2] H.Y. Sohn, J. Szekely, Reactions between solids through gaseous intermediates-I reactions controlled by chemical kinetics, Chem. Eng. Sci. 28 (10) (1973) 1789–1801.
[3] O.I. Nokhrina, I.D. Rozhihina, I.E. Hodosov, The use of coal in a solid phase reduction of iron oxide IOP Conference Series: Mate. Sci. Eng. 91 (2015) 012045, https://doi.org/10.1088/1757-899X/91/1/012045.
[4] N.S. Srinivasan, Reduction of iron oxides by carbon in a circulating fluidized bed reactor, Powder Technol. 124 (1-2) (2002) 28–39.
[5] R. Sah, S.K. Dutta, Kinetic studies of iron ore-coal composite pellet reduction by TG–DTA, Trans. Indian Inst. Met. 64 (6) (2011) 583–591.
[6] C.E. Seaton, J.S. Foster, J. Velasco, Redution kinetics of hematite and magnetite pellets containing coal char, Transactions of the Iron and Steel Institute of Japan 23 (6) (1983) 490–496.
[7] K. Ma, J. Deng, G. Wang, Q.i. Zhou, J. Xu, Utilization and impacts of hydrogen in the ironmaking processes: A review from lab-scale basics to industrial practices, Int. J. Hydrogen Energy 46 (52) (2021) 26646–26664.
[8] D. Spreitzer, J. Schenk, Reduction of iron oxides with hydrogen—a review, steel research int. 90 (10) (2019) 1900108, https://doi.org/10.1002/srin.v90.1010.1002/srin.201900108.
[9] E.R. Monazam, R.W. Breault, R. Siriwardane, Kinetics of hematite to wüstite by hydrogen for chemical looping combustion, Energy Fuels 28 (8) (2014) 5406–5414.

[10] H.-B. Zuo, C. Wang, J.-J. Dong, K.-X. Jiao, R.-S. Xu, Reduction kinetics of iron oxide pellets with H2 and CO mixtures, Int. J. Miner. Metall. Mater. 22 (7) (2015) 688–696.
[11] Q. Tang, Y. Ma, K. Huang, Fe3O4/ZrO2 Composite as a robust chemical looping oxygen carrier: a kinetics study on the reduction process, ACS Applied Energy Materials 4 (7) (2021) 7091–7100.
[12] J. Dang, K.-C. Chou, X.-J. Hu, G.-H. Zhang, Reduction kinetics of metal oxides by hydrogen, steel research int. 84 (6) (2013) 526–533.
[13] A.A. Barde, J.F. Klausner, R. Mei, Solid state reaction kinetics of iron oxide reduction using hydrogen as a reducing agent, Inter. J. Hydrogen Energy 41 (24) (2016) 10103–10119.
[14] S.-H. Kim, X. Zhang, Y. Ma, I.R. Souza Filho, K. Schweinar, K. Angenendt, D. Vogel, L.T. Stephenson, A.A. El-Zoka, J.R. Mianroodi, M. Rohwerder, B. Gault, D. Raabe, Influence of microstructure and atomic-scale chemistry on the direct reduction of iron ore with hydrogen at 700°C, Acta Mater. 212 (2021) 116933, https://doi.org/10.1016/j.actamat.2021.116933.
[15] Z. Chen, J. Dang, X. Hu, H. Yan, Reduction kinetics of hematite powder in hydrogen atmosphere at moderate temperatures, Metals 8 (10) (2018) 751.
[16] S.S. Jung, J.S. Lee, In-situ kinetic study of hydrogen reduction of fe2o3 for the production of fe nanopowder, Mater. Trans. 50 (2009) 2270–2276.
[17] T. Zhang, C. Lei, Q. Zhu, Reduction of fine iron ore via a two-step fluidized bed direct reduction process, Powder Technol. 254 (2014) 1–11.
[18] Damien Wagner, O. D., Fabrice Patisson, Denis Ablitzer, A Laboratory Study of the Reduction of Iron Oxides by Hydrogen. *In 2006 TMS Fall Extraction and Processing Division: Sohn International Symposium* **2006,** *2*, 111-120.
[19] K. Piotrowski, K. Mondal, T. Wiltowski, P. Dydo, G. Rizeg, Topochemical approach of kinetics of the reduction of hematite to wüstite, Chem. Eng. J. 131 (1-3) (2007) 73–82.
[20] W.C. Cho, D. Lee, C.H. Kim, H.S. Cho, S.D. Kim, Feasibility study of the use of by-product iron oxide and industrial off-gas for application to chemical looping hydrogen production, Appl. Energy 216 (2018) 466–481.
[21] J.R. Scheffe, M.D. Allendorf, E.N. Coker, B.W. Jacobs, A.H. McDaniel, A. W. Weimer, Hydrogen production via chemical looping redox cycles using atomic layer deposition-synthesized iron oxide and cobalt ferrites, Chem. Mater. 23 (8) (2011) 2030–2038.
[22] J.-B. Yang, N.-S. Cai, Z.-S. Li, Hydrogen production from the steam−iron process with direct reduction of iron oxide by chemical looping combustion of coal char, Energy Fuels 22 (4) (2008) 2570–2579.
[23] X. Zhao, Y.H. Gong, X. Li, N.S. Xu, K. Huang, Cyclic durability of a solid oxide fe-air redox battery operated at 650 degrees C, J. Electrochem. Soc. 160 (10) (2013) A1716–A1719.
[24] X. Zhao, X. Li, Y. Gong, N. Xu, K. Huang, A novel intermediate-temperature all ceramic iron–air redox battery: the effect of current density and cycle duration, RSC Adv. 4 (43) (2014) 22621–22624.
[25] C. Zhang, K. Huang, An intermediate-temperature solid oxide iron-air redox battery operated on o2--chemistry and loaded with pd-catalyzed iron-based energy storage material, ACS Energy Lett. 1 (6) (2016) 1206–1211.
[26] C. Zhang, K. Huang, MOF-derived iron as an active energy storage material for intermediate-temperature solid oxide iron–air redox batteries, Chem. Commun. 53 (76) (2017) 10564–10567.
[27] N. Xu, C. Zhang, K. Huang, Proton-mediated energy storage in intermediate-temperature solid-oxide metal–air batteries, J. Mater. Chem. A 6 (42) (2018) 20659–20662.
[28] A.M. Jubb, H.C. Allen, Vibrational spectroscopic characterization of hematite, maghemite, and magnetite thin films produced by vapor deposition, ACS Appl. Mater. Interfaces 2 (10) (2010) 2804–2812.
[29] B. Gunawardana, N. Singhal, P. Swedlund, Degradation of chlorinated phenols by zero valent iron and bimetals of iron: a review, Environ. Eng. Res. 16 (4) (2011) 187–203.
[30] A. Goikhman, P. Shvets, U. Koneva, R. Mantovan, K. Maksimova, Polycrystalline magnetite (Fe3O4) thin films from FeOx/Fe bilayers grown by pulsed laser depositions, Thin Solid Films 652 (2018) 28–33.
[31] M. Fanfoni T. M., The Johnson-Mehl-Avrami-Kolmogorov model: A brief review Il Nuovo Cimento D 20 7 1998 1171 1182.
[32] R.M.S. Haiming Liu, J.C. Hanson, C.P. Grey, J.D. Martin, Kinetics and mechanism of the b to a cualcl4 phase transition: a time-resolved 63cu mas nmr and powder x-ray diffraction study, J. Am. Chem. Soc. 123 (2001) 7564–7573.
[33] M.C. Weinberg, D.P. Birnie, V.A. Shneidman, Crystallization kinetics and the JMAK equation, J. Non-Cryst. Solids 219 (1997) 89–99.
[34] R. Lück, K. Lu, W. Frantz, JMA analysis of the transformation kinetics from the amorphous to the nanocrystalline state, Scr. Metall. Mater. 28 (9) (1993) 1071–1075.
[35] E. Lorente, J. Herguido, J.A. Peña, Steam-iron process: Influence of steam on the kinetics of iron oxide reduction, Int. J. Hydrogen Energy 36 (21) (2011) 13425–13434.
[36] K. Piotrowski, K. Mondal, H. Lorethova, L. Stonawski, T. Szymanski, T. Wiltowski, Effect of gas composition on the kinetics of iron oxide reduction in a hydrogen production process, Int. J. Hydrogen Energy 30 (15) (2005) 1543–1554.
[37] P. Pourghahramani, E. Forssberg, Reduction kinetics of mechanically activated hematite concentrate with hydrogen gas using nonisothermal methods, Thermochim Acta 454 (2) (2007) 69–77.
[38] E.R. Monazam, R.W. Breault, R. Siriwardane, Reduction of hematite (Fe2O3) to wüstite (FeO) by carbon monoxide (CO) for chemical looping combustion, Chem. Eng. J. 242 (2014) 204–210.